Electronic Supporting Information

Enhancement of charge-assisted hydrogen bond capabilities due to O-alkylation proximity in alkoxy cationic polythiophenes: solution- and solid-state evidence via EPR, AFM and surface free energy

Sergio E. Domínguez*†, Antti Vuolle,† Alberto Fattori,‡ Timo Ääritalo,† Michela Cangiotti,‡ Pia Damlin,† M. Francesca Ottaviani‡ and Carita Kvarnström†

†*Turku University Centre for Materials and Surfaces (MATSURF), Laboratory of Materials Chemistry and Chemical Analysis, University of Turku, 20014 Turku, Finland*
‡*Department of Pure and Applied Sciences (DiSPeA), University of Urbino, Via Ca' Le Suore 2/4, 61029 Urbino, Italy*
*Corresponding author: sergioedominguez@gmail.com

1. Solvents and co-solvation

Water and W-DI have both densities of ≈1 g/cm^3, however these solvents have clearly different values of Hildebrand's H-bonding capacity, viscosity and dielectric constant (see Table 1). These extent of variation in their properties makes W-DI a useful system, as shown by previous studies in solution and/or solid states, by our[1 2 3 4 5] and other[6 7 8] groups, and also in applied research focused on organic optoelectronics.[9 10] Density functional theory (DFT) have shown that DI disrupts the H-bonding donor-acceptor ratio of water, that can disrupt the normal structure of water, allowing the modulation of complexing, because of its relatively bulky structure consisting of ether groups, capable of accepting two hydrogen bonds, without donating any.[11] Molecular dynamics (MD) have been used to analyze the selective solvation of anionic oligomers in W-DI, in comparison with water,[12] allowing to sketch a qualitative explanation of the co-solvation present in the system. Notice that these authors (and also our previous works)[3 4] labeled such selective solvation as a DI "coating effect". Experimental evidence of the phenomena occurrng in the W-DI solvent was reported by Luong et al.,[13] who analyzed the dynamics of H-bonded collective networks in water-DI mixtures. It was observed that heteromolecular H-bonding between water and DI dominates only in the water diluted region, while the progressive

addition of water, above a mole fraction of 0.1, generates a bulk-like, intermolecular, three-dimensional H-bonded water network dynamics. The selective solvation of CPEs in binary mixtures has been analyzed at a qualitative level only, since quantitative analyses require empirical solvation data to estimate solute-solvent parameters. Such empirical data is not available for CPTs, CPEs or even hydrophobic conjugated polymers (CPs). This is clearly exemplified in the work by Burrows et al.[12]

2. Qualitative approach to study solvation & co-solvation of ionic molecules

In the present work, the use of W-DI causes co-solvation to play a central role on the solution interactions under study. This is not a trivial phenomenon, especially when considering the ionic nature of the donor-acceptor pair, which jeopardizes the possibility to perform quantitative studies on solvation/co-solvation, which are out of the scope of the present work.

Previous studies on the solubility of bare (neutral, non-ionic) C_{60}, like those performed by Marcus et al.[14] or Cysewski[15] rely on datasets of physical and chemical solubility properties (e.g. the Kamlet-Taft hydrogen bond donicity), estimated (empirically or computationally) from a large variety of solvents. These datasets are then analysed using methods such as multivariate stepwise linear regression or a consonance solvents approach, in order to describe mechanistically (and predict) the solubility of C_{60}. To our knowledge, there are not datasets like these focused on water-soluble fullerenes, cationic polythiophenes (CPTs), or any other conjugated polyelectrolyte (CPEs).

Another quantitative approach is the use of the Hansen solubility parameters, which split interfacial energies into dispersive, polar, and H-bonding components. This approach also been used to analyze solubility/miscibility of bare C_{60}, using data from a broad selection of solvents and *non-conjugated* polymers, in the context of donor-acceptor pairs in organic photovoltaics.[16] However, there are not datasets like these focused neither in neutral (hydrophobic) conjugated polymers (CPs), nor in water-soluble fullerenes, CPTs or CPEs in general. The review by Yao and Tam[17] shows how only qualitative solvation analyses have been used in studies involving stimuli-responsive water-soluble (C_{60})polymers.

Besides this lack of empirical datasets from hydrophilic fullerenes and polymers, the use of binary solvent mixtures further compromise the possibility of performing quantitative studies on solvation. As stated in the review by Homocianu and Airinei,[18] the photophysical properties of solutes when dissolved in mixed solvents are influenced by the composition of systems (e.g. repartitioning of the cosolvent between solvation shell and bulk phase) and also by the intermolecular interactions that can be present (e.g. H-bonding, charge transfer, molecular associations, dipole–dipole and dipole–induced dipole interactions). As a consequence, the physicochemical properties of many solvatochromic probes in binary solvents often show large deviations from the ideal behavior, as shown by the small correlation coefficients of microenvironment polarity (evaluated by Lippert–Mataga, Bakhshiev and Kawski–Chamma–Viallet polarity functions) observed for some fluorinated poly(oxadiazole-ether)s.[18]

This lack of correlation of the Lippert-Mataga function has also been reported for CPEs in binary solvent systems, as reviewed by Burrows et al.,[19] on a study using DI as a cosolvent to break up clusters of an anionic CPE,[12] in which it was not possible to correlate spectral shifts with dielectric constant, either directly or with the Onsager or Lippert-Mataga functions. The data showed a poor correlation with the microscopic solvation parameter, however, a trend was observed in emission maxima with the parameter, suggesting that there is some specific interaction between the cosolvent and the polymer chromophoric component (i.e. the CPE backbone). MD simulations confirmed this assumption, showing preferential solvation of the backbone by the DI cosolvent, a “coating” displacing water from the immediate environment of the molecule, while the ionic parts are preferentially solvated by water, reducing interchain and side-chains interactions, in comparison with the system in water.[19]

The review by Marcus on the co-solvation of drugs in binary solvent mixtures,[20] is a perfect example on why a quantitative approach on co-solvation is beyond the scope of the present work, and the whole field of CPEs, to this date.

3. EPR methodology

EPR spectra were recorded by an EMX-Bruker spectrometer operating at X band (9.5 GHz) and interfaced with a PC (software from Bruker for handling and recording the EPR spectra). The temperature was controlled by a Bruker ST3000 variable temperature assembly cooled with liquid nitrogen. The reproducibility was verified by repeating each experiment at least three times.

For the spin probes, the concentration of 0.05 mM was selected for all probes because it showed to be non-perturbative of the systems on the basis of the invariability of the spectral line shape by further decreasing this concentration. On the other hand, 0.25 mM is known to generate aggregates of the CPTs (further details on the polymeric solutionsa ahead).

The computation of the spectra was accomplished by means of the well-established procedure of Budil et al.[21] The EPR spectral line shape is determined by the molecular reorientational dynamics of the spin probe and its constraints over correlation times ranging from 10-11 to 10-6 s. According to the Kubo-Tomita theory, it is possible to simulate EPR spectra on the basis of peculiar dynamic models.[21] Anisotropies of the reorientational motion of anisotropic molecules, e.g., nitroxide molecules, mainly surfactants, were accounted for by introducing simple potentials. A modification of the Levenberg–Marquardt minimization algorithm was used for the analysis of the EPR spectra. The dynamic parameters describing the slow motion are obtained from least-squares fitting of model calculations based on the stochastic Liouville equation (SLE) to experimental spectra. The correlation time obtained provides a measure of microviscosity at the nitroxide site.

The main parameters extracted from computation were (i) the Aii components of the hyperfine coupling tensor A for the coupling between the electron spin and the nitrogen nuclear spin. These components measure the environmental polarity. Unless otherwise specified, for simplicity, the Axx and Ayy components were assumed constant (6 G), whereas only Azz was changed. The accuracy of this parameter is ±0.01 G; (ii) the correlation time for the diffusional rotation motion of the probe (τ), which measures the microviscosity around the probe, in turn monitoring the interactions occurring

among the molecules at the probe site. The accuracy in this parameter is ±1 ps.[22] The total intensity of well reproducible EPR spectra was evaluated by the double integral of the spectra in arbitrary units (A.U.). Quantitative EPR measurements of spin concentration cannot be performed in the absence of an internal reference, but, in the present case, we trusted the intensity values only in a comparative way for a series of samples, for an indirect measure of the spin-probe solubility.

Some typical EPR spectra are shown in Figures S-1 to S-5 ahead.

4. Polymeric solutions

The CPTs were dissolved in water until a concentration of 0.478 mg/mL and stirred for 30 min, in order to obtain a 0.48 mg/mL (2 mM, monomer base) aqueous solution. Stock solutions in water and the W-DI mixture were then obtained by duplicating the volume of the 0.48 mg/mL aqueous solution, either with water or DI. The obtained 0.24 stock solutions have the highest polymer concentrations used in this work. The solutions at low polymer concentration, 0.1 mM, were obtained by diluting each stock solution either with water or with a W-DI mixture. These concentrations were used since PT1 is known to be aggregated and disaggregated, at 0.24 mg/mL (1 mM) and 0.024 (0.1 mM), respectively.[2] The conformational evolution and aggregation processes of polymer chains is a very slow process, probably related with their molecular weight, as shown in studies with methoxyethoxy polythiophenes.[23] This is in agreement with the absorbance−fluorescence spectroscopic features of aqueous solutions of PT1, which showed to be stable during at least 2 months (results not shown). Regardless, in the present study fresh stock solutions obtained from the same original water 2 mM solution were used.

5. Drop-casted films on mica and atomic force microscopy (AFM)

The films were obtained by drop-casting 3 μL of 1 mM (0.24 mg/mL) solutions of PT1, either in water or W-DI, on freshly cleaved mica surfaces. This concentration was selected after the work by Kesters et

al., using cationic polythiophenes.[24] The solutions were filtered through a 5-6 μm PTFE membrane, to minimize the possible presence of dust particles. The drops were allowed to dry at ambient temperature in a sealed container overnight. The AFM measurements were performed in a class 100 clean room, under ambient conditions, in tapping mode, using silicon cantilevers (≈225 nm length, ≈20 nm tip-height, resonance frequency ≈84 kHz). The AFM micrographs were processed with aid of the freeware Gwyddion.[25]

6. Production of the spin coated films onto glass

Spin-coated CPTs-films were deposited either from water or W-DI, on air-plasma-cleaned microscope borosilicate glass coverslips (VWR International). Air-plasma decreases the number of siloxane groups while increasing the surface concentration of H-bonding donor OH groups,[26] thus increasing the value of the "silanol number".[27] Besides the CPTs, the plasma-activated glass slips were spin-coated only with water or DI, in order to obtain the "glass/water" and "glass/DI" blanks respectively.

The polymeric films were produced by adding 3 μL of 0.2 mg/mL solutions of each CPT (for concentrations ≈0.7-0.8 mM), dissolved either in water or W-DI, on an already 500 rpm-spinning substrate (i.e. dynamic dispense). This is the range of concentration used in our previous contribution,[3] chosen following previous studies from our group to produce self-assembled multilayers (0.25 mg/mL),[28] and also the previously mentioned studies of Kesters et al.,[24] which reports that concentrations of 0.25 mg/mL (in methanol) showed to be optimal to observe differences in OSCs efficiencies as a function of the cationic functionality in the polythiophene.

In order to maximize reproducibility (i.e. decrease experimental error) all films were produced from the same batch solutions and by the same operator. In order to minimize biased data due to the learning curve of the process, the production of films and the CA measurements were randomized as much as possible by avoiding systematical production or measuring of films exposed to the same treatment (i.e. same polymer or processing solvent) or similar measurements (e.g. same probe liquids).

7. Relevance of surface free energy in opto- and bio-electronic applications

Some mechanistic explanations have been proposed to explain the role of films of CPEs in organic electronics, using Kelvin probe force microscopy (KPFM) or ultraviolet photoelectron spectroscopy (UPS) and/or direct evaluation of OSCs devices. Besides these techniques, the surface free energy (SFE) also provides structural information of polymeric films. SFE and surface-potential govern the adhesion and interaction energies of CPs-films,[29] [30] and can be estimated using contact angle (CA) goniometry. This method is relatively simpler than other techniques for SFE estimation (e.g. inverse gas chromatography), however it provides high sensitivity.[31] SFE is relevant for opto- and bio-electronics because it governs (together with the surface-potential) the adhesion and interaction energies of CPs-films.[29] [30] Adhesion also impacts the mechanical stability and long-term reliability of polymeric films applied to OSCs. [32] [33] SFE also impacts the miscibility between the components within the active layer,[34] [35] or between adjacent layers[35] [36] [37] in OSCs. Adhesion between films and biomolecules (e.g. DNA, serum protein or cells) plays a central role in bioelectronics.[29] [30] [38] A recent study reported that a quaternary-ammonium CPT improved the biofilm formation and extracellular electron transport of a polymer–exoelectrogen hybrid bioelectrode.[39] A dithiophene-benzothiadiazole CPE showed capabilities as electron acceptor from *Shewanella oneidensis*, promoting cell coverage, in bioelectrochemical systems (BESs).[40] [41] SFE is also convenient since it estimates the polar and dispersive contributions of the surface energy, and for surfaces with identical surface energy, that with a higher value of the polar contribution, will induce higher degree of cell adhesion and proliferation on the surface.[38]

8. Methodology for SFE estimations

The SFE estimations with Wu's method were obtained considering the four probe liquids shown in Table S-2 (glycerol, ethylene glycol, formamide and diiodomethane).[42] The calculations to estimate the

SFE were performed with the aid of the software KSV Surface Free Energy Analysis (version 3.0), copyright KSV Instruments, Ltd (1997-2005), using the averages of at least triplicate CA measurements from different experimental units.

In this work, CA between blank surface or CPTs-films and different probe liquids (glycerol, ethylene glycol, formamide, and diiodomethane) were measured using the sessile drop method, with 3 μL drops of each probe liquid. The CA value was taken from the stabilized reading. The surface tension values of the respective liquids (γL), and their constituting polar and dispersive forces (γLp and γLd, respectively) are shown in Table S-2. Notice that surface tension of liquids and SFE of solids are commonly reported in literature either with units of force/unit length (mN/m) or energy/unit area (mJ/m2), with both scales being numerically equivalent.

Table S-1. Values of physical-chemical parameters relevant for the studies, from all the solvents (at 20° or 29° C). There are also shown, the H-bonding capacities of each pure solvent (according to the Hildebrand scale), and the values of the H-bonding interactive force (δH) of the Hansen solubility parameters of each pure solvent. Next to each value is provided the number of the reference

Solvent	***Density (g/cm3)***	***Dynamic viscosity (mPa s)***	***Dielectric constant***	***Refractive index***	***Boiling point (°C)***
Water	0.99 [43]	*0.754 [44]	80.38 [45]	*1.33 [44]	100
W-DI	1.03 [46]	*1.4 [44]	36.89 [45]	*1.40 [44]	87.82[47] †

*At 29 C°

†For a mixture with 46.91% DI

Table S-1-cont.

Solvent	***H-bonding capacity ****	***δD Dispersion †***	***δP Polar †***	***δH Hydrogen bonding †***
Water	Strong	15.5	16.0	42.3
DI	Moderate	17.5	1.8	9.0

∗ [48]

† [49]

Table S-2. Total surface tension (γL) of the probe liquids used in this work, together with their constituting dispersive (γL^d) and polar (γL^p) contributions.

	Glycerol	Ethylene glycol	Formamide	Diiodomethane
γL (mN/m)	63.4	47.7	58.2	50.8
γL^d (mN/m)	37	26.4	39.5	48.5
γL^p (mN/m)	26.4	21.3	18.7	2.3

Table S-3. CA values of all the blanks and PT1 films with the four probe liquids used. For the values of PIM' please see the supplementary information of our previous work [3] (in which PIM' is labeled as PIMb).

	Blanks			PT1 0.2 mg/mL		PT2 0.2 mg/mL		PIMa 0.2 mg/mL	
	glass/water	glass/DI	plasma	Water	W-DI	Water	W-DI	Water	W-DI
Glycerol	42.41	48.7	43.18	31.60	47.99	54.02	34.90	32.35	26.64
	47.05	49.0	44.62	34.11	45.20	48.08	38.85	28.77	28.62
	32.32	42.2	31.31	41.18	40.92	40.62	41.24	31.11	31.98
	35.79	37.9	31.12	46.36	34.24	40.95			
						44.80			
Average	**39.39**	**44.44**	**37.56**	**38.31**	**42.09**	**45.69**	**38.33**	**30.74**	**29.08**
SD	6.6	5.39	7.35	6.73	5.99	5.57	3.20	1.82	2.70
RSD	16.76	12.13	19.57	17.56	14.23	12.19	8.35	5.91	9.29
Ethylene-glycol	24.17	29.31	22.87	32.09	29.72	31.72	31.98	8.43	16.81
	32.92	33.10	30.35	33.23	29.39	27.85	26.50	10.51	14.68
	27.10	27.73	18.96	24.90	19.12	31.16	25.94	17.77	18.10
	18.60		17.43	26.54	32.78	28.55		12.73	
	24.57		19.75	26.56		31.44			
	16.89			25.87					
				28.73					
Average	**24.04**	**30.05**	**21.87**	**28.27**	**27.75**	**30.14**	**28.14**	**12.36**	**16.53**
SD	5.82	2.76	5.14	3.23	5.953	1.80	3.34	4.01	1.73
RSD	24.20	9.19	23.49	11.41	21.45	5.98	11.86	32.46	10.47
Forma-mide	13.89	17.36	9.72	20.52	18.32	22.06	19.90	15.92	8.47
	16.15	18.63	4.40	20.16	17.33	22.12152	17.67245566	15.70	7.15
	13.16	16.86	6.65	19.63	13.26	19.24	22.00	15.81	10.98
		14.20	7.60		11.87	20.73			
			7.78			19.05			
						17.60			
Average	**14.40**	**16.76**	**7.23**	**20.10**	**15.19**	**20.13**	**19.86**	**15.81**	**8.87**
SD	1.56	1.87	1.94	0.45	3.12	1.81	2.16	0.11	1.95
RSD	10.81	11.15	26.78	2.232	20.50	9.01	10.90	0.69	21.96
Diiodo-methane	41.46	42.94	39.78	25.88	32.16	25.84	28.85	25.85	26.12
	43.97	47.10	38.23	27.21	37.50	31.04	42.97	27.57	31.02
	44.24	42.55	37.03	31.82	41.05	30.97	42.92	28.79	38.43
	38.20	40.82	33.28	29.80	27.12	36.04		31.67	
	48.23		37.41	34.17		40.30			
			45.01						
Average	**43.22**	**43.35**	**38.46**	**29.78**	**34.46**	**32.84**	**38.24**	**28.47**	**31.85**
SD	3.71	2.66	3.86	3.362	6.11	5.52	8.13	2.45	6.20
RSD	8.58	6.14	10.05	11.29	17.73	16.79	21.27	8.613	19.45

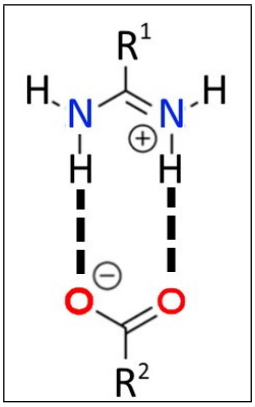

Scheme S-1. Scheme of the $R_2^2(8)$ hydrogen bonding geometry, often observed in *charge-assisted H-bond* frameworks, modified from [50].

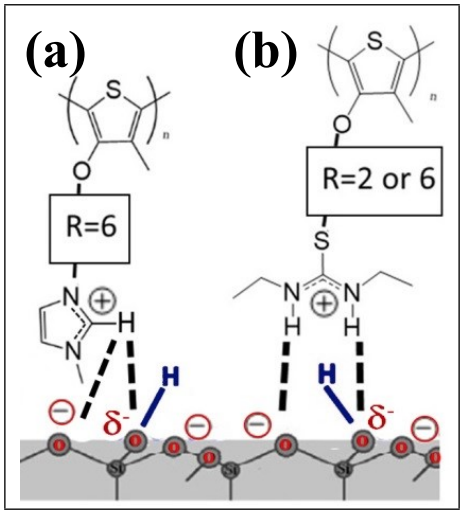

Scheme S-2. Expected interactions between plasma-activated glass or mica with the CPEs used in this work: (a) with the imidazolium group in PIMa (pi+) and (b) with the isothiouronium group in PT1 or PT2 via two-point +CAHB (modified from Matisons,[51] Wu et al., [52] Pouryousefy et al. [53] and, in regard to the two-point $R_2^2(8)$ hydrogen bonding geometry, Boer et al.[50] Notice that both the –OH and Si-O-Si groups present in plasma-glass and mica are shown, being partially negative (δ) in the –OH groups present in plasma-glass, and negative for the case of Si-O-Si groups present in mica and partially on plasma-glass. Blue hydrogens indicate the –OH groups expected in plasma-activated glass (i.e. silanol number).

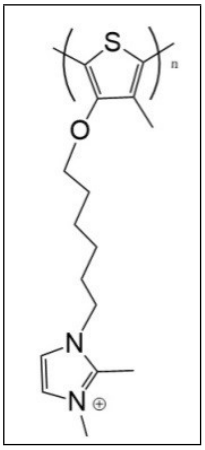

Scheme S-3. Skeletal structure of PIM'

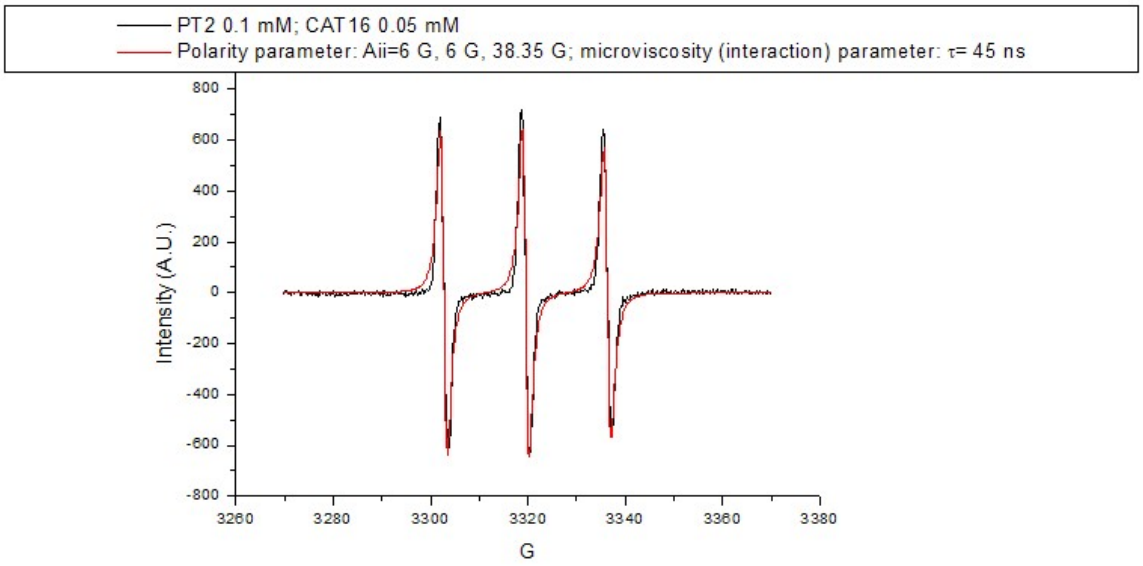

Figure S-1. Example of experimental and computed EPR spectra for the probe CAT16 (0.05 mM) in solution with PT2 (0.1 mM). The main parameters used for computation are also reported in the figure.

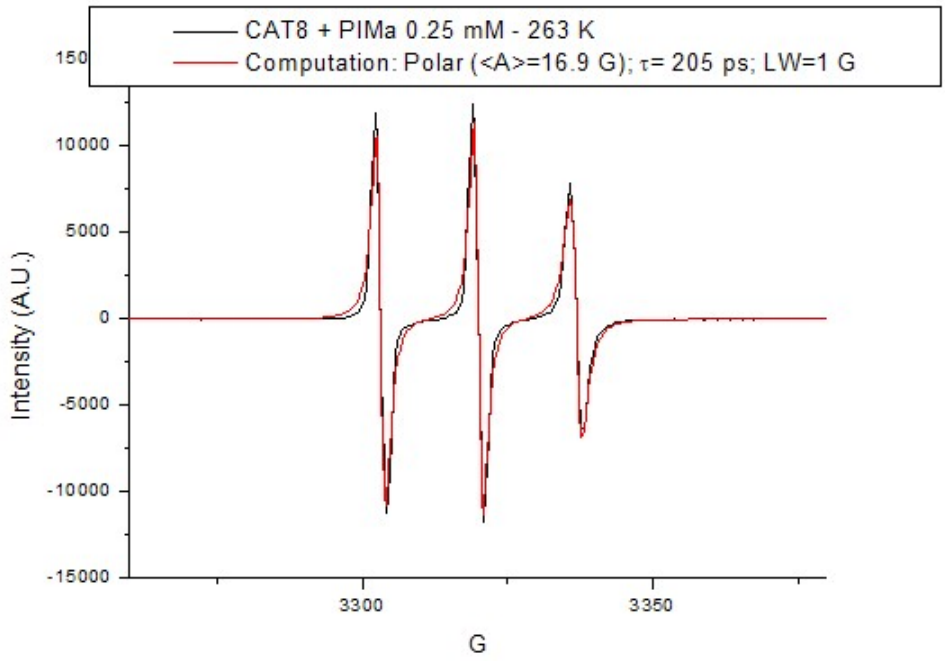

Figure S-2. Example of experimental and computed EPR spectra for the probe CAT8 (0.05 mM) in solution with PIMa (0.25 mM). The main parameters used for computation are also reported in the figure.

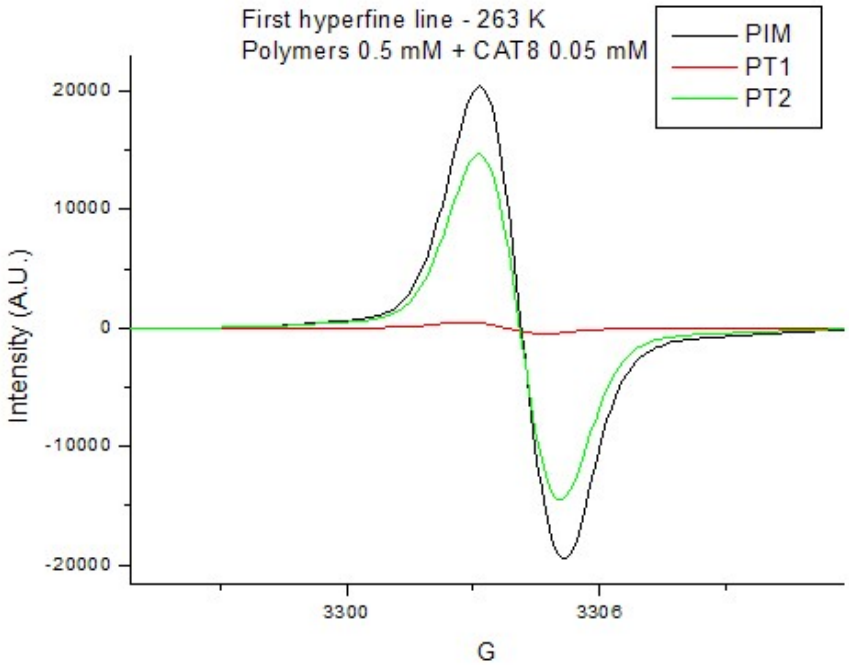

Figure S-3. Figure 7: First hyperfine line of the spectra of CAT8 in solution of the polymers PIMa, PT1 and PT2 at 263.

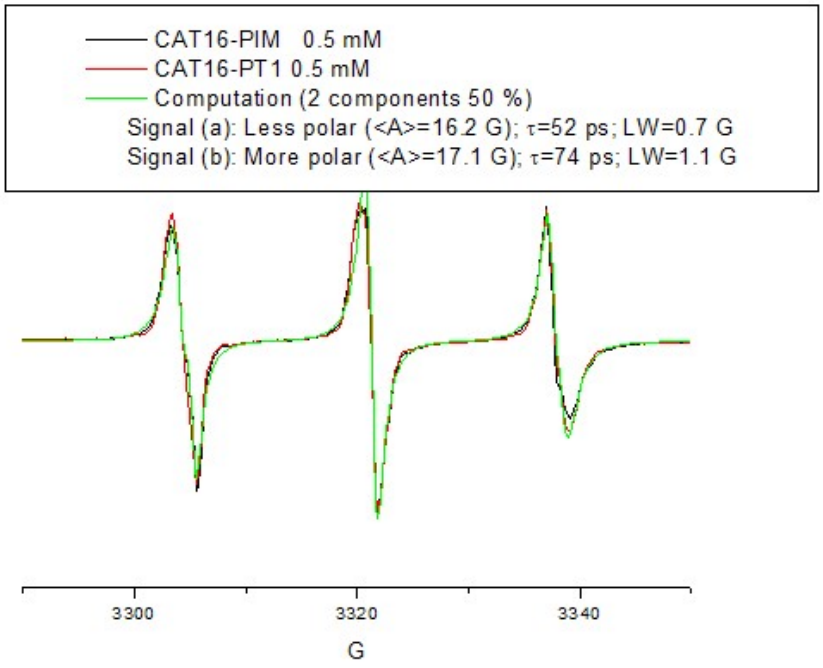

Figure S-4. Experimental and computed spectra for CAT16 in PIM and PT1 at 0.5 mM (263 K). Computation was obtained by adding two spectral components at about 50 %: Signal (a): Free less polar (present for all polymers) and Signal (b): Free more polar (present for all polymers).

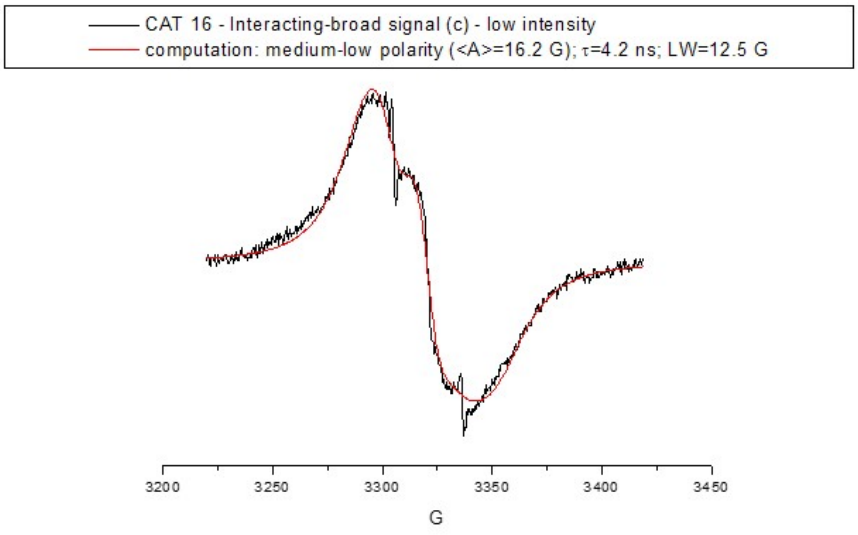

Figure S-5. Experimental and computed Signal: Interacting-broad component (present for all polymers with the exclusion of PT1, at very low relative intensity: about 15 %), obtained by subtracting the other two components from the experimental spectra.

References

1 S. E. Domínguez, M. Meriläinen, T. Äaritalo, P. Damlin and C. Kvarnström, *RSC Adv.*, 2017, **7**, 7648–7657.
2 S. E. Domínguez, M. Cangiotti, A. Fattori, T. Ääritalo, P. Damlin, M. F. Ottaviani and C. Kvarnström, *Langmuir*, 2018, **34**, 7364–7378.
3 S. E. Domínguez, A. Vuolle, M. Cangiotti, A. Fattori, T. Äaritalo, P. Damlin, M. F. Ottaviani and C. Kvarnström, *Langmuir*, 2020, **36**, 2278–2290.
4 S. E. Domínguez, A. Vuolle, C. Butler-Hallissey, T. Ääritalo, P. Damlin and C. Kvarnström, *Journal of Colloid and Interface Science*, 2021, **584**, 281–294.
5 S. E. Domínguez, B. Kohn, T. Äaritalo, P. Damlin, U. Scheler and C. Kvarnström, *Phys. Chem. Chem. Phys.*, 2021, **23**, 21013–21028.
6 P. Bhavya, R. Melavanki, R. Kusanur, K. Sharma, V. T. Muttannavar and L. R. Naik, *Luminescence*, 2018, **33**, 933–940.
7 H. Yao, S. Sugiyama, R. Kawabata, H. Ikeda, O. Matsuoka, S. Yamamoto and N. Kitamura, *J. Phys. Chem. B*, 1999, **103**, 4452–4456.
8 H. Yao, Y. Morita and K. Kimura, *Journal of Colloid and Interface Science*, 2008, **318**, 116–123.
9 T. Nakagawa, J. Hatano and Y. Matsuo, *J. Porphyrins Phthalocyanines*, 2014, **18**, 735–740.
10 S. Chen, Z. Liu and Z. Ge, *Polymer Journal*, 2016, **48**, 101–110.
11 M. R. Kris, PhD thesis, Washington State University, 2010.
12 H. D. Burrows, S. M. Fonseca, C. L. Silva, A. A. C. C. Pais, M. J. Tapia, S. Pradhan and U. Scherf, *Phys. Chem. Chem. Phys.*, 2008, **10**, 4420–4428.
13 T. Q. Luong, P. K. Verma, R. K. Mitra and M. Havenith, *J. Phys. Chem. A*, 2011, **115**, 14462–14469.
14 Y. Marcus, A. L. Smith, M. V. Korobov, A. L. Mirakyan, N. V. Avramenko and E. B. Stukalin, *J. Phys. Chem. B*, 2001, **105**, 2499–2506.
15 P. Cysewski, *Symmetry*, 2019, **11**, 828.
16 C. M. Hansen and A. L. Smith, *Carbon*, 2004, **42**, 1591–1597.
17 Z. Yao and K. C. Tam, *Macromolecular Rapid Communications*, 2011, **32**, 1863–1885.
18 M. Homocianu and A. Airinei, *Journal of Molecular Liquids*, 2015, **209**, 549–556.
19 H. D. Burrows, M. Knaapila, S. M. Fonseca and T. Costa, in *Conjugated Polyelectrolytes*, John Wiley & Sons, Ltd, 2013, pp. 127–167.
20 Y. Marcus, *Pharmaceutica Analytica Acta*, , DOI:10.4172/2153-2435.1000537.
21 D. E. Budil, S. Lee, S. Saxena and J. H. Freed, *Journal of Magnetic Resonance Series A*, 1996, **120**, 155–189.
22 M. F. Ottaviani, M. Cangiotti, L. Fiorani, A. Barnard, S. P. Jones and D. K. Smith, *New J. Chem.*, 2012, **36**, 469–476.
23 J. Zhu, Y. Han, R. Kumar, Y. He, K. Hong, P. V. Bonnesen, B. G. Sumpter, S. C. Smith, G. S. Smith, I. N. Ivanov and C. Do, *Nanoscale*, 2015, **7**, 15134–15141.
24 J. Kesters, S. Govaerts, G. Pirotte, J. Drijkoningen, M. Chevrier, N. Van Den Brande, X. Liu, M. Fahlman, B. Van Mele, L. Lutsen, D. Vanderzande, J. Manca, S. Clément, E. Von Hauff and W. Maes, *ACS Applied Materials and Interfaces*, 2016, **8**, 6309–6314.
25 D. Nečas and P. Klapetek, *centr.eur.j.phys.*, 2012, **10**, 181–188.
26 L. Dalstein, E. Potapova and E. Tyrode, *Physical Chemistry Chemical Physics*, 2017, **19**, 10343–10349.
27 L. T. Zhuravlev, *Langmuir*, 1987, **3**, 316–318.

28 A. Viinikanoja, S. Areva, N. Kocharova, T. Ääritalo, M. Vuorinen, A. Savunen, J. Kankare and J. Lukkari, *Langmuir*, 2006, **22**, 6078–6086.
29 M. J. Higgins and G. G. Wallace, *Polymer Reviews*, 2013, **53**, 506–526.
30 M. J. Higgins, P. J. Molino, Z. Yue and G. G. Wallace, *Chem. Mater.*, 2012, **24**, 828–839.
31 P. A. Hunt, C. R. Ashworth and R. P. Matthews, *Chem. Soc. Rev.*, 2015, **44**, 1257–1288.
32 S. R. Dupont, E. Voroshazi, P. Heremans and R. H. Dauskardt, *Organic Electronics*, 2013, **14**, 1262–1270.
33 A. Gusain, R. M. Faria and P. B. Miranda, *Front. Chem.*, , DOI:10.3389/fchem.2019.00061.
34 N. D. Treat, M. A. Brady, G. Smith, M. F. Toney, E. J. Kramer, C. J. Hawker and M. L. Chabinyc, *Advanced Energy Materials*, 2011, **1**, 82–89.
35 R. Singh, S. R. Suranagi, J. Lee, H. Lee, M. Kim and K. Cho, *Scientific Reports*, 2018, **8**, 2849.
36 M. Kim, J. Lee, S. B. Jo, D. H. Sin, H. Ko, H. Lee, S. G. Lee and K. Cho, *J. Mater. Chem. A*, 2016, **4**, 15522–15535.
37 S. Kouijzer, J. J. Michels, M. van den Berg, V. S. Gevaerts, M. Turbiez, M. M. Wienk and R. A. J. Janssen, *J. Am. Chem. Soc.*, 2013, **135**, 12057–12067.
38 L. Chen, C. Yan and Z. Zheng, *Materials Today*, 2018, **21**, 38–59.
39 P. Zhang, X. Zhou, R. Qi, P. Gai, L. Liu, F. Lv and S. Wang, *Advanced Electronic Materials*, 2019, **5**, 1900320.
40 L. Ren, S. R. McCuskey, A. Moreland, G. C. Bazan and T.-Q. Nguyen, *Biosensors and Bioelectronics*, 2019, **144**, 111630.
41 N. D. Kirchhofer, S. R. McCuskey, C.-K. Mai and G. C. Bazan, *Angewandte Chemie International Edition*, 2017, **56**, 6519–6522.
42 Thomsen, F., 2008.
43 V. Belandria, A. H. Mohammadi and D. Richon, *Journal of Chemical Thermodynamics*, 2009, **41**, 1382–1386.
44 J. Nayak, M. Aralaguppi, B. V. Naidu and T. Aminabhavi, *J. Chem. Eng. Data*, 2004, **49**, 468–474.
45 F. E. Critchfield, J. A. Gibson Jr. and J. L. Hall, *Journal of the American Chemical Society*, 1953, **75**, 1991–1992.
46 L.-M. Omota, O. Iulian, F. Omota and O. Ciocirlan, *Revue Roumaine de Chimie*, 2009, **54**, 63–73.
47 E. R. Smith and M. Wojciechowski, *Journal of Research of the N.ational Bureau of Standards*.
48 A. F. M. Barton, *CRC Handbook of Solubility Parameters and Other Cohesion Parameters, Second Edition*, CRC Press, Second., 1991.
49 C. M. Hansen, *Hansen Solubility Parameters: A User's Handbook, Second Edition*, 2007.
50 S. A. Boer, P.-X. Wang, M. J. MacLachlan and N. G. White, *Crystal Growth & Design*, 2019, **19**, 4829–4835.
51 J. G. Matisons, in *Silicone Surface Science*, eds. M. J. Owen and P. R. Dvornic, Springer Netherlands, Dordrecht, 2012, pp. 281–298.
52 J. Wu, F. Liu, H. Yang, S. Xu, Q. Xie, M. Zhang, T. Chen, G. Hu and J. Wang, *Journal of Industrial and Engineering Chemistry*, 2017, **56**, 342–349.
53 E. Pouryousefy, Q. Xie and A. Saeedi, *Petroleum*, 2016, **2**, 215–224.